LANGMUIR Article
Cite This: Langmuir 2019, 35, 16734−16744
pubs.acs.org/Langmuir

Mechanical Properties of DPPC−POPE Mixed Langmuir Monolayers

Alberto S. Luviano,[†] José Campos-Terán,[‡] Dominique Langevin,[§] Rolando Castillo,[∥] and Gabriel Espinosa*[,†]

[†]Instituto de Física y Matemáticas, Universidad Michoacana de San Nicolás de Hidalgo, 58060 Morelia, México
[‡]Departamento de Procesos y Tecnología, Universidad Autónoma Metropolitana, Unidad Cuajimalpa, 05348 Ciudad de México, México
[§]Laboratoire de Physique des Solides, Université Paris-Sud, 91405 Orsay, France
[∥]Instituto de Física, Universidad Autónoma de México, P.O. Box 20-264, 01000 Ciudad de México, México

Supporting Information

ABSTRACT: The mechanical properties of lipid monolayers and their responses to shear and compression stresses play an important role in processes such as breathing and eye blinking. We studied the mechanical properties of Langmuir monolayers of a model mixture, composed of an unsaturated lipid, 1-palmitoyl-2-oleoyl-*sn*-glycero-phosphoethanolamine (POPE), and a saturated lipid, 1,2-dipalmitoyl-*sn*-glycero-phosphocholine (DPPC). We performed isothermal compressions and sinusoidal shear deformations of these mixed monolayers. Also, the different phases were observed with Brewster angle microscopy. We found that the mechanical behavior is affected by the miscibility of both lipids. In the two-phase region, the compression elastic modulus increases with the amount of the LC phase but does not follow the predictions of a simple effective medium model. The discrepancies arise from the fact that, upon compression, the domains grow at a rate faster than the compression rate but not fast enough to reach thermodynamic equilibrium. Before reaching the LC phase, domain percolation is observed and compression and shear moduli become equal to those of the pure LC phase. Most of the monolayers behave as viscoelastic fluids at the frequencies investigated. A minimum in the compression modulus and shear viscosity was observed for mixtures close to equimolar composition, with the minimum being accompanied by a change in domain shapes.

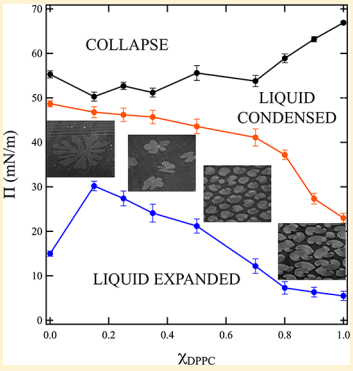

INTRODUCTION

Understanding the physical properties of lipid bilayers is closely related to the biological function of cells.[1,2] Lipid bilayers provide mechanical stability to the membranes as well as a fluid environment allowing proteins and other molecules to move along or across these membranes. The bilayers are composed of mixtures of lipids with saturated and unsaturated chains in order to be able to modulate the cell mechanical response to various types of stresses. In the breathing process, the lung cell membranes are exposed to huge changes in surface pressure; in the eye blinking process, the lipid surface layer experience a shear stress every 2−10 s.[3] Mixed lipid monolayers have proven to be adequate models to tackle cell membrane mechanics.[4] However, few such studies have been published so far, although they could bring important insights and innovation, for instance in medical treatments of diseases related to dry eye and breathing deficiencies.[5] Important advances in the understanding of the mechanical behavior of lipid monolayers were published recently.[6] This motivated us to undertake a study of mixtures of saturated and unsaturated lipids.

Depending on the particular lipid and on temperature, the mechanical response of mixed lipid monolayers is rather complex. Pure lipids and lipid mixtures usually present a so-called *liquid expanded* (LE) phase at low surface pressure and a *liquid condensed* (LC) phase at high surface pressure, separated by a phase coexistence region.[7] The surface pressure is not constant in the coexistence region, a feature that attracted much interest in the past and was first attributed to impurities.[8] More recently, the role of the liquid condensed domains nucleating in the LE phase was considered. When the domains are not able to incorporate material freely during compression, the monolayer is not in thermodynamic equilibrium, and the compression modulus is not equal to zero as in the thermodynamic limit; the faster the compression, the larger the delay in domain growth, the higher the modulus and the closer the behavior to that of a composite with rigid elements. Such composites are usually described by effective medium theories.[9] In their simplest version, the compressibility (inverse of elastic compression modulus) of the mixed monolayers is the sum of the compressibility of each coexisting phase weighted by the percentage of area occupied by each phase. In these models, the linear elasticity of heterogeneous materials is not sensitive to the details of the microstructure, and in particular to anisotropy.[10]

Received: September 23, 2019
Revised: November 17, 2019
Published: December 2, 2019

DOI: 10.1021/acs.langmuir.9b02995
Langmuir 2019, 35, 16734−16744

Such a description was applied recently to lipid mixtures by Caruso et al. in the region of LE−LC coexistence.[6] Although the compression modulus was nonzero, the effective medium theory failed to describe their results. In addition, a percolation behavior was observed close to the LC phase, where the LC domains become macroscopically connected and the measured modulus becomes equal to the modulus of the LC phase. Similar approaches were used to describe the shear rheology of lipid monolayers; this problem is simpler because the area of the domains remains constant during a shear deformation. The shear viscosity of mixed lipid monolayers has been modeled in analogy with three-dimensional suspensions of hard spheres in a solvent, and a perfect agreement has been obtained with no adjustable parameters.[11]

Apart from the study of Caruso et al.,[6] few studies of mechanical behavior of mixed lipid monolayers have been reported to date. In a former work, we have studied the shear behavior of several representative mixed lipid monolayers composed solely of saturated lipids and evidenced a wide range of behavior, from fluid to viscoelastic and solid, depending on composition.[12] Wilke et al. studied the shear behavior of mixed monolayers of DSPC (distearoylphosphatidylcholine) and DMPC (dimystroylphophatidylcholine).[13] The monolayer shear viscosity was found to be highly dependent on the presence of domains and on the domain density. In turn, the monolayer compressibility was only influenced by the presence of domains for high domain densities, as confirmed later by the work of the same group.[6] Work is clearly needed to deepen our understanding of the mechanical behavior of mixed monolayers, in particular containing unsaturated lipids, which are adequate models of cell membrane mechanics.

The diversity of lipid composition is enormous and is even different in the inner and outer monolayers of membrane bilayers.[14] In the present study, we have chosen a model system with two lipids, DPPC and POPE (Figure 1). DPPC,

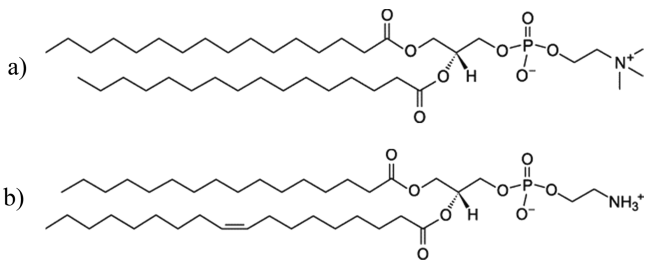

Figure 1. (a) DPPC and (b) POPE chemical structures.

1,2-dipalmitoyl-*sn*-glycero-3-phosphocholine, is a common component of lung cell membranes. DPPC is a saturated lipid and its transition temperature is 41 °C.[15] Monolayers and bilayers of this lipid have been widely studied, including their mechanical properties.[15−20] POPE, 1-palmitoyl-2-oleyl-*sn*-glycero-3-phosphoethanolamine, is unsaturated and its transition temperature is 25 °C. This lipid increase bilayer fluidity, because it has a low transition temperature[21] and also because the amine in the headgroup is not methylated.[22,23] Monolayer studies of the two pure lipids could be found in the literature, especially for DPPC.[15−20]

In the present paper, we intend to clarify the mechanical response of mixed lipid monolayers containing DPPC, a saturated lipid, and POPE, an unsaturated one. We studied the miscibility and the mechanical response to both compression and shear deformations of the mixed monolayers.

MATERIALS AND METHODS

Materials. The lipids 1,2-dipalmitoyl-*sn*-glycero-3-phosphocholine (DPPC, M_W = 734, cat. 850355P) and 1-palmitoyl-2-oleyl-*sn*-glycero-phosphoethanolamine (POPE, M_W = 718, cat. 850757P) were purchased from Avanti Polar Lipids (Alabaster, AL). According to the supplier, DPPC is an L-enantiomer. All chemicals were used as received. We prepared stock solutions of each lipid in chloroform (supplied by Sigma-Aldrich, St. Louis, MO) at a concentration of 1 mg/mL. We mixed the DPPC and POPE lipid solutions with different mole fractions of DPPC, χ_{DPPC}. All stock solutions were kept at −20 °C. We formed Langmuir monolayers by spreading a small amount (20 μL) of the lipid solutions dropwise, with a microsyringe (Hamilton Co.) onto a clean subphase of ultrapure water (Milli-Q, Millipore with a resistivity of 18.2 MΩ·cm). The cleanliness of the water/air interface was tested by compressing the interface (by a factor ∼4), checking that the change in surface tension was less than 0.2 mN/m and that no domains were observed with Brewster angle microscopy (BAM). Prior to all measurements, we waited 20 min to allow for chloroform evaporation.

Surface Compression Isotherms and Compression Modulus. The surface tension was measured with a tensiometer (KSV-NIMA, KN 0051) equipped with a Du Nouy−Padday platinum rod (KSV-NIMA, KN 0004, diameter of 3.317 mm). The surface pressure is defined as $\Pi = \gamma_0 - \gamma$, where γ_0 is the surface tension of water and γ is the surface tension in the presence of the monolayer. Compression isotherms, Π vs area per molecule a, were performed in a Langmuir trough (KSV-NIMA, KN 3003) with area 364 mm × 75 mm at a low compression rate (3.75 cm^2/min), in order to be close to quasi-static conditions. In the case of lipid mixtures, a was calculated dividing the trough area by the total number of molecules deposited at the surface.

The temperature was controlled by recirculating water from a thermostatic bath (Thermo Scientific). The temperature, T, was measured using a thermocouple (KSV-NIMA, KN0054) immersed in the water subphase. In the experiments presented in this paper, T = (20 ± 0.02)°C. The Langmuir trough was placed inside a transparent plexiglass box to avoid undesired air drift and dust contamination on the liquid surface. This box was set on a table equipped with an active vibration isolation system (Accurion, Vario Basic 40). The surface compression modulus (E) was obtained from numerical derivatives of $\Pi(a)$:

$$E = -a\left(\frac{\partial \Pi}{\partial a}\right) \quad (1)$$

It is known the unsaturated lipids are prone to oxidation. Their double bonds are susceptible to break during oxidation reactions in the presence of reactive oxygen species,[24] accelerated in the presence of ozone.[25] We investigated the oxidation of POPE lipids in the laboratory atmosphere by monitoring the time evolution of surface pressure. No significant variations were detected less than 90 min after monolayer formation, while the surface pressure begins to change appreciably at elapsed times of 150 min (Figure S1). None of our experiments lasted more than 80 min; therefore, we considered unnecessary the use of an oxygen-free atmosphere.

Brewster Angle Microscopy (BAM). The textures of the lipid monolayers were observed using an Elli2000 (Nanofilm Technologie GmbH, Germany) imaging ellipsometer in microscopy mode. The instrument is equipped with a p-polarized laser beam with an incidence angle of ∼53° onto the air/water interface and a CCD detector to collect the reflected light, with a 20× objective (field of view: 292 μm × 235 μm and a spatial resolution of ∼1 μm per pixel).

Interfacial Shear Rheology (ISR). We used a KSV-NIMA interfacial shear rheometer (ISR).[26,27] The instrument features two Helmholtz coils producing a magnetic field gradient in order to displace a millimetric magnetic needle. The needle has a magnetic core of 7.3 mg inserted in a hollow glass capillary with 23 mm length and 0.4 mm diameter. The magnetic needle is carefully placed onto

DOI: 10.1021/acs.langmuir.9b02995
Langmuir 2019, 35, 16734−16744

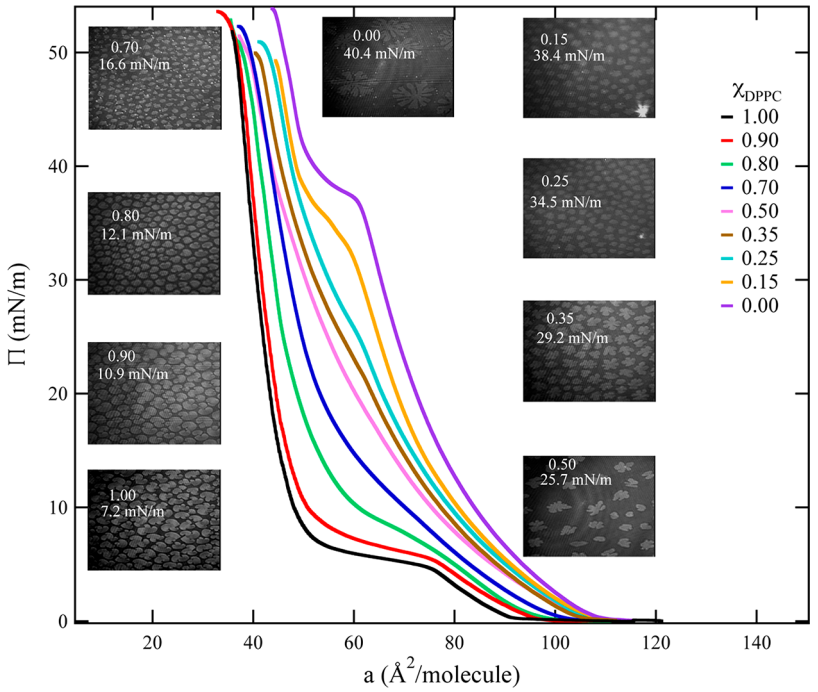

Figure 2. Surface pressure Π−*a* isotherms of lipid mixtures of POPE−DPPC with different DPPC molar fractions χ_{DPPC}. BAM images are taken in the LE−LC coexistence region; the values of χ_{DPPC} and of the pressures are indicated in each image; the horizontal length of the images is 292 μm.

the air/water interface covered by the spread monolayer in the Langmuir trough. The needle slides inside a glass channel that creates a small wetting meniscus, which is used as a guide for the needle to move along a straight line parallel to the walls of the channel, ensuring uniform flow geometry. The barriers of the Langmuir trough were set to motion automatically in order to maintain constant the monolayer surface pressure during the shear deformation. All the ISR measurements were performed at a constant low angular frequency from $\omega = 0.13\ s^{-1}$ and using small amplitudes (<5%) in order to remain in the linear viscoelastic regime. Three different measurements were performed in order to evaluate the reproducibility.

The sinusoidal shear stress, σ, applied to the magnetic needle writes:

$$\sigma(t) = \sigma_0 \sin(\omega t + \delta) \tag{2}$$

The stress amplitude, σ_0, is measured after force calibration. The strain amplitude, denoted by u_0, is deduced from the displacement of the magnetic needle.[26,28] When the monolayer is purely elastic, the phase difference δ is zero, while when the monolayer is purely viscous, $\delta = \pi/2$. The complex viscoelastic surface modulus was obtained from

$$G^*(\omega) = \frac{\sigma_0}{u_0} e^{i\delta(\omega)} = G'(\omega) + iG''(\omega) \tag{3}$$

where $G'(\omega)$ is the storage modulus and $G''(\omega)$ is the loss modulus. G'' is related to the surface shear viscosity η_s by $G'' = \omega \eta_s$. When $G' = 0$ and $G'' \neq 0$, the surface layer is fluid with a viscosity η_s; when $G' \neq 0$ and $G'' = 0$, the layer is purely elastic; when both G' and G'' are nonzero, the layer is viscoelastic.[29]

RESULTS AND DISCUSSION

Surface Pressure and Phase Transitions. The surface pressure isotherms of mixed POPE−DPPC monolayers are shown in Figure 2 for different DPPC molar fractions (χ_{DPPC}).

The isotherms for monolayers of pure lipids are similar to those reported in the literature.[30,31] The pure DPPC isotherm is characterized by a liquid expanded (LE) phase at large molecular area. The surface pressure increases during the compression of the LE phase up to the appearance of a liquid condensed (LC) phase after a characteristic kink at *ca.* 5 mN/m.[32] In the LE−LC coexistence region, the surface pressure is not constant and increases slowly. Upon further compression, only the LC phase remains and the surface pressure rises sharply until the monolayer collapses. Adding POPE to DPPC monolayers results in an increase of surface pressure (for a given area per molecule). The kink at the onset of LE−LC phase coexistence is less marked, and the curve gradually shifts toward higher pressures as χ_{DPPC} decreases. The pure POPE isotherm exhibits the largest surface pressures, and again a marked kink in the surface pressure at the onset of LE−LC phase coexistence. The kink occurs at a much higher surface pressure (~38 mN/m) than in DPPC monolayers (~5 mN/m).[31] This is because monolayers of unsaturated lipids are less compressible than saturated ones (their transition temperature is lower).

Brewster angle images of the monolayers were taken between Π ~ 0 (LE phase) and the monolayer collapse. Above Π = 5 mN/m, triskelion-shaped LE−LC domains are observed in pure DPPC monolayers, while above 38 mN/m, seaweed-shaped domains are observed in pure POPE monolayers. The same type of domain shapes has been observed in previous studies of the pure lipid monolayers.[33,34] Upon decreasing χ_{DPPC}, the domains evolve progressively from triskelion-like toward seaweed-like (Figure 2 insets). DPPC domains form triskelions at high surface concentrations, evolving from a bean-like shape at low surface concentrations.[35] Additional images can be found in Figure S2. These domains are usually not at equilibrium and grow during compression; their shape is therefore controlled by the growth process. At low supersaturation, they are affected by instabilities occurring during domain growth, where Marangoni flow is the key factor.[36,37] Here, the domains in DPPC monolayers present the characteristic chirality of L-enantiomers.[38] Upon POPE addition, above ca. $\chi_{DPPC} \approx 0.70$, the

DOI: 10.1021/acs.langmuir.9b02995
Langmuir 2019, 35, 16734−16744

domains grow without apparent orientational order, as when the line tension of the domains does not present anisotropy.

The pressure Π_e at the onset of appearance of the LC phased the pressure Π_c above which the domains disappear were determined using the BAM images and are reported in Table 1. We also report in this table the surface pressure of the kink (Π_k) observed in the isotherms. As expected, Π_e and Π_k, are equal within experimental error, except for the pure POPE monolayers (see Table 1). In this case, small nucleation seeds appear at a pressure of ca. 15 mN/m, much smaller than Π_k, as also observed by other authors.[31] The increase in Π_k with addition of POPE is expected as the transition temperature of the monolayer decreases: the mixed monolayers become more expanded and less compressible. Π_k was found to vary linearly with χ_{DPPC} as Π_e (excepted for pure POPE) (see Figure S3).

Table 1. Surface Pressures (in mN/m) at the Onset of Formation of the Liquid Condensed Domains (Π_e) and at which the domains disappear (Π_c), determined using BAM images, and Surface Pressure at the Kink of the Isotherms (Π_k) for Different DPPC Molar Fractions

χ_{DPPC}	Π_e	Π_k	Π_c
0.00	14.9 ± 0.6	37.6 ± 0.6	48.8 ± 0.7
0.15	33 ± 1	33.1 ± 0.9	47 ± 1
0.25	26 ± 1	25 ± 1.0	46 ± 2
0.35	22 ± 2	22 ± 1	46 ± 2
0.50	18 ± 2	17 ± 1	44 ± 2
0.70	12 ± 1	11 ± 1	41 ± 2
0.80	8.0 ± 0.7	7 ± 1	37 ± 1
0.90	5.8 ± 0.4	6 ± 1	27 ± 1
1.00	5.2 ± 0.2	4.6 ± 0.8	23 ± 1

The slope of the isotherms decreases and the width of the coexistence region increases as χ_{DPPC} approaches 0.5, the value for the equimolar mixture. This means that the monolayer becomes more compressible in the vicinity of χ_{DPPC} = 0.5 and that according to eq 1 the effective modulus E is minimum, as discussed later.

A phase diagram can then be constructed for a given surface pressure, the two χ values at which the boundaries of each homogeneous region are crossed can be determined and are plotted in Figure 3.

Relative Area Occupied by the Surface Domains. The area occupied by the domains in the coexistence regions was determined using image analysis with the NIH ImageJ[39] software as detailed in the Supporting Information. The area A_c and A_e occupied by respectively the LC and LE phases were determined using the BAM images for all χ_{DPPC}. The variation of condensed area fraction $A_c/(A_c + A_e)$ with surface pressure is shown in Figure 4 for the different χ_{DPPC}.

The area covered by the condensed phase increases rapidly with surface pressure and saturates at high surface pressures, before but close to the monolayer collapse. At a fixed surface pressure, the fraction of condensed area decreases with addition of POPE.

As in the study of Caruso et al.,[6] we tested if the lever rule was obeyed, meaning that the composition of the coexisting phases does not change in the coexistence region. This rule writes:

$$\frac{A_e}{A_c} = \frac{a_e\chi_c - \chi_{DPPC}}{a_c\chi_{DPPC} - \chi_e} \quad (4)$$

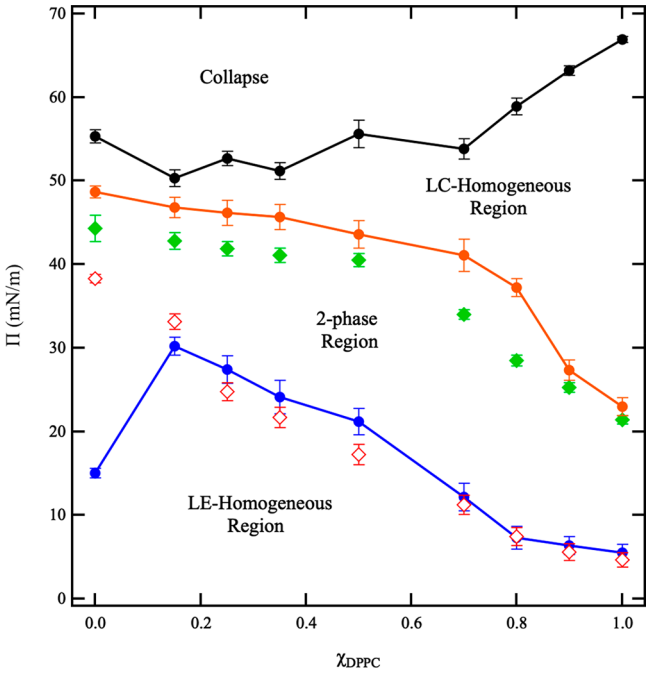

Figure 3. Phase diagram of the mixed monolayers. A homogeneous LE region is found under the blue line ($\Pi = \Pi_e$), a two-phase region between the blue line and the orange line ($\Pi = \Pi_c$), and a collapse region above the black line. The pressure at which domain percolation occurs is also shown (green squares), as well as the pressure of the kink ($\Pi = \Pi_k$, (empty red diamonds). Except for Π_k and the collapse line, the points were obtained from BAM image analysis.

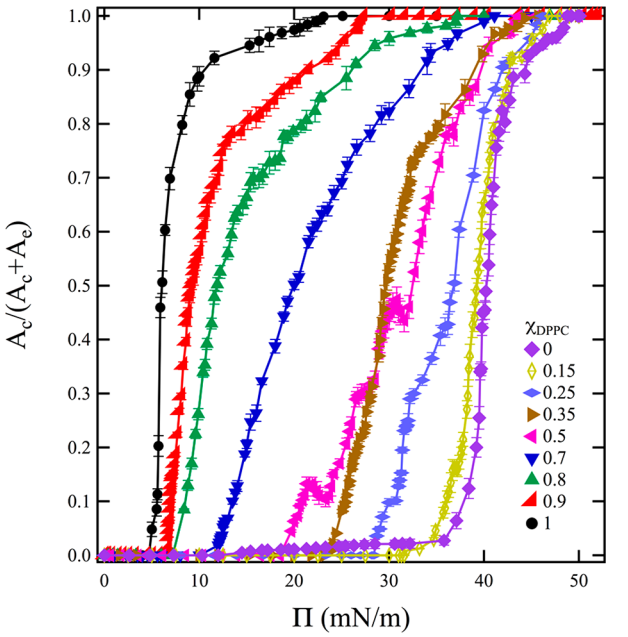

Figure 4. Relative area covered by the LC phase for different monolayer compositions, obtained from analysis of BAM images; A_c and A_e are respectively the surface area of condensed and the expanded phases.

where χ_e and χ_c are, respectively, the molar fractions of DPPC in the expanded and condensed phases, obtained from the phase diagram of Figure 3, while a_e and a_c are respectively the mean molecular area of the expanded and condensed phases, obtained from the compression isotherms of Figure 2 at the

DOI: 10.1021/acs.langmuir.9b02995
Langmuir 2019, 35, 16734−16744

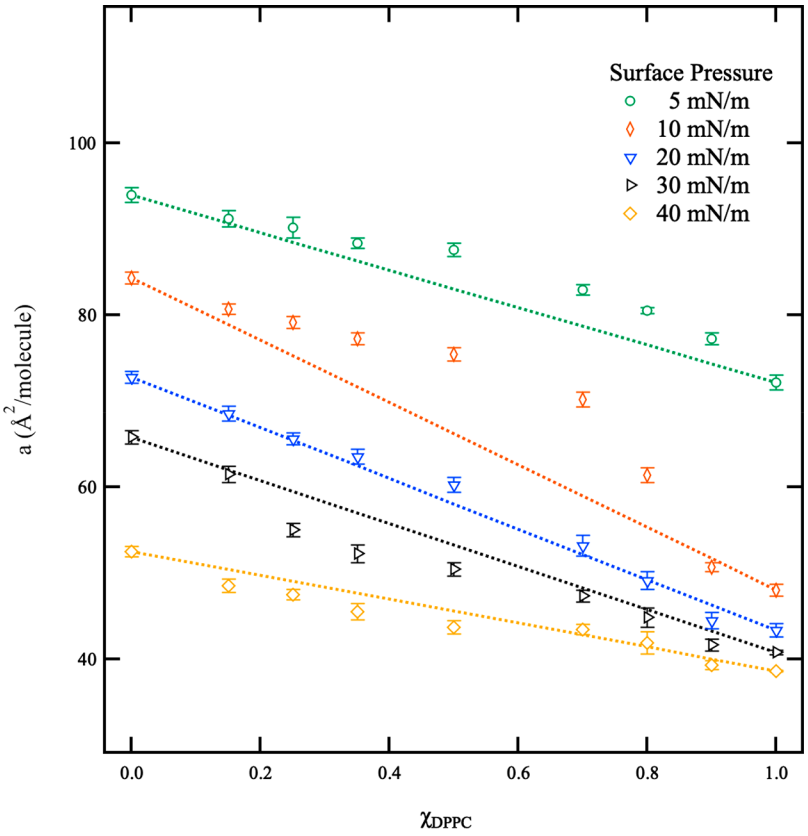

Figure 5. Mean molecular area dependency of DPPC molar fraction. The dashed lines represent the prediction of an ideal mixture.

compositions χ_e and χ_c. The experimental data for χ_e, χ_c, a_e, and a_c corresponding to surface pressures of 15, 20, 30, and 35 mN/m together with the curves calculated using eq 4 are presented in the Supporting Information (Figure S4). We found that the lever rule is obeyed in the monolayers of this study, meaning that at constant surface pressure, the composition of the coexisting phases does not change.

We also evaluated the average size of the domains from image analysis. It does not depend appreciably on surface pressure, but increases slightly with χ_{DPPC} from about 10 μm for small χ_{DPPC} to 20 μm for large χ_{DPPC}.

Gibbs Excess Free Energy of Mixing. Figure 5 shows the area per lipid (a) at fixed pressures versus χ_{DPPC}, determined using the isotherms of Figure 2. For an ideal mixture:

$$a_{ideal}(\chi) = \chi_{DPPC} a_{DPPC} + (1 - \chi_{DPPC}) a_{POPE} \quad (5)$$

This linear behavior is not obeyed by the mixed monolayers as it can be seen in Figure 5. Values larger than predicted from eq 5 would indicate that the effective area per molecule is greater than the ideal area, a more loosely packed state regardless the monolayer phase state, and lower values would indicate a more compact monolayer than the ideal one. Also on each surface pressure the mean molecular area decreases monotonically, the largest deviations from the ideal area occurs at Π = 10 mN/m.

To evaluate the interaction between lipids in the monolayer and its stability, we calculate the Gibbs excess free energy, ΔG_{exc}, determined from the following relation:[40,41]

$$\Delta G_{exc} = \int_0^{\Pi} (a_{mix} - \chi_{DPPC} a_{DPPC} - (1 - \chi_{DPPC}) a_{POPE})\, d\Pi \quad (6)$$

where a_{mix}, a_{DPPC}, and a_{POPE} represent the real area of mixed system and the respective areas of pure components. In the pure component monolayer, ΔG_{exc} = 0, this is also true if the mixed monolayers has an ideal behavior. If the monolayer present $\Delta G_{exc} < 0$, meaning that the interaction between mixed components is more attractive, whereas $\Delta G_{exc} > 0$, it indicates a more repulsive interaction between the two species. In Figure S5, we observe that ΔG_{exc} is positive for most of the mixtures at the selected surface pressures (5, 10, 20, 30, and 40 mN/m), therefore the miscibility of both lipids is not favorable except for surface pressures of 30 and 40 mN/m and $\chi_{DPPC} \approx 0.9$, where $\Delta G_{exc} < 0$, in these conditions we observed an LC homogeneous monolayer (see Figures 5 and S2).

Compression Modulus. The compression modulus (E) obtained from numerical derivation of the isotherms using eq 1 is shown in Figure 6. At low surface pressures (~5 mN/m, LE phase), the compression modulus is low, E < 50 mN/m, indicating that all the monolayers are quite compressible, pure DPPC being the most compressible monolayer of all of them ($E \sim 5$ mN/m). At high surface pressures ($\Pi \sim 40$ mN/m), close to the LC phase, the pure POPE monolayer is in turn the most compressible and presents the smallest E value of the monolayers in this study. The curve of Figure 6 has been smoothed numerically in order to reduce the noise. As a consequence, the discontinuities associated with the kinks of surface pressure are not visible. The moduli at the phase transitions were calculated without smoothening.

At intermediate surface pressures, E decreases with addition of POPE until χ_{DPPC} = 0.5, after which it does not significantly change upon further addition of POPE. If we assume that the monolayer behaves as an effective medium in the two-phase region, the compression modulus should obey:

DOI: 10.1021/acs.langmuir.9b02995
Langmuir 2019, 35, 16734−16744

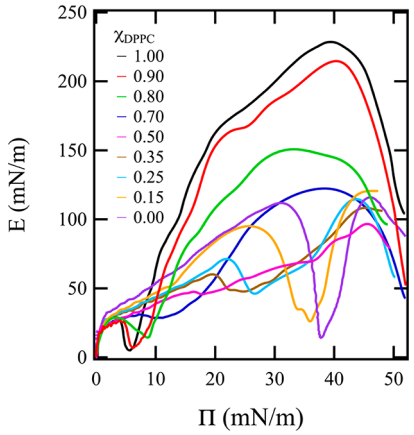

Figure 6. Smoothened curve for the compression modulus (E) vs the surface pressure for monolayers of different DPPC/POPE mixtures.

$$E^{-1} = -\frac{1}{A}\left(\frac{\partial(A_e + A_c)}{\partial \Pi}\right) = \frac{1}{A}\left(\frac{A_e}{E_e} + \frac{A_c}{E_c}\right) \quad (7)$$

where E_c is the compression modulus of the condensed phase and E_e is the compression modulus of the expanded phase. The values of E_e were obtained from the derivatives of the surface pressure at the kink on the high surface area side. The values of E_c were obtained from the derivatives of the surface pressure at Π_c (since in this case, there is no visible discontinuity in surface pressure). These values are given in Table 2 for the different χ_{DPPC}.

Table 2. Calculated Compression Moduli E_c and E_e (in mN/m) at the Transition Pressures Reported in Table 1 for Different DPPC Molar Fractions

χ_{DPPC}	E_e	E_c
0.00	67 ± 3	102 ± 6
0.15	53 ± 3	119 ± 6
0.25	65 ± 4	110 ± 5
0.35	54 ± 4	112 ± 5
0.50	49 ± 3	89 ± 4
0.70	28 ± 4	121 ± 7
0.80	20 ± 3	147 ± 8
0.90	24 ± 3	175 ± 8
1.00	27 ± 3	177 ± 7

The plots of $1/E$ versus $x = A_c/A$ are shown in Figure 7. Portions of linear behavior can be visualized, suggesting that the monolayers might behave as an effective medium, at least within the error bars. However, when $1/E$ is calculated using the values of E_e and E_c of Table 2 and eq 7, large discrepancies are found with the experimental data (red lines in Figure 7). This means that effective medium models are unable to describe the compression behavior of the monolayers, as reported earlier.[6,9] The difference is unusually large for pure DPPC monolayers, which exhibits a marked kink at the LE−LC transition when arriving at the LE phase; the modulus is thus much smaller in the two-phase region than in the pure LE phase close to the kink, a feature not accounted for by eq 7.

It can be seen in Figure 7 that although the compression elastic modulus increases with the amount of LC phase, it increases less than predicted by a simple effective medium model. This mismatch arises from the fact that upon compression, the domains grow at a rate faster than the compression rate, but not fast enough to reach thermodynamic equilibrium, in which case the modulus should be zero.

The modulus becomes constant, and equal to E_c before reaching the liquid-condensed phase ($x = 1$), suggesting that the domains percolate and become interconnected over macroscopic distances, as confirmed by the examination of the BAM images. The same behavior was found for other lipids by Caruso et al.[6] To better visualize this effect, we normalized the compression moduli in order to compare their behavior for different χ_{DPPC}. Each modulus was normalized according to

$$E_{norm} = \frac{E - E_e}{E_c - E_e} \quad (8)$$

The results are shown in Figure 8.

The values of $x = A_c/A$ at the percolation threshold, above which the normalized elastic modulus becomes close to one and rather constant, are given in Table 3. The percolation threshold does not depend significantly upon χ_{DPPC} although a slight increase is observed between pure POPE and pure DPPC. The values of the percolation threshold determined from the BAM images are also given in Table 3. Within experimental error, they agree with the values taken from the elastic modulus. Percolation is shifted to smaller surface pressures by increasing χ_{DPPC} (see Figure 3). Note that Caruso et al.[6] found differences between percolation thresholds determined from BAM images and elastic moduli of their lipids; they proposed that the domains appearing in contact in the images were not yet connected.

The values of the percolation threshold either from BAM images and from elastic moduli displayed in Table 3 are large, significantly larger than the 2D percolation thresholds that correspond to close packing for disks or aligned squares, which are about 0.67.[42] The percolation threshold is larger for elongated objects, but also depends on the interactions between surface domains. These large values were also observed by Caruso et al. and were attributed to these domain interactions.

The smallest compression modulus values are found for $\chi_{DPPC} \approx 0.3-0.5$. Figure 9 shows this effect for three different pressures, mostly for monolayers in the two-phase region ($\Pi_e < \Pi < \Pi_c$). Also, as surface pressure increases, the minimum is clearly seen at lower χ_{DPPC}.

Note that for $\chi_{DPPC} = 0.5$, there is no kink in the surface pressure isotherm (Figure 2) and that at this composition, the domain shapes change from seaweed to triskelion-like, which could be related to the change in the line tension due to the interaction between lipids.

The compressibility E_c^{-1} corresponding to the monolayers just entering the condensed phase (Figure 9 and Table 2) is also maximum at $\chi_{DPPC} = 0.5$, implying that this homogeneous LC monolayer is also the most compressible one. Following the self-assembly model of Israelachvili et al.[43,44] and since DPPC and POPE molecules have respectively cone and inverted-cone geometries[45] (close to cylinders), one can understand why the equimolar mixture has an optimal molecular packing, therefore, the pair interactions might be maximized at a given density. The mean molecular area, a, in Figure 5 shows that at $\chi_{DPPC} \approx 0.5$ and lower surface pressures ($\Pi \leq 20$ mN/m) there is the highest positive deviation from the ideal mixture (dashed lines in Figure 5), suggesting that at these surface pressures and this molar fraction the monolayer is

DOI: 10.1021/acs.langmuir.9b02995
Langmuir 2019, 35, 16734−16744

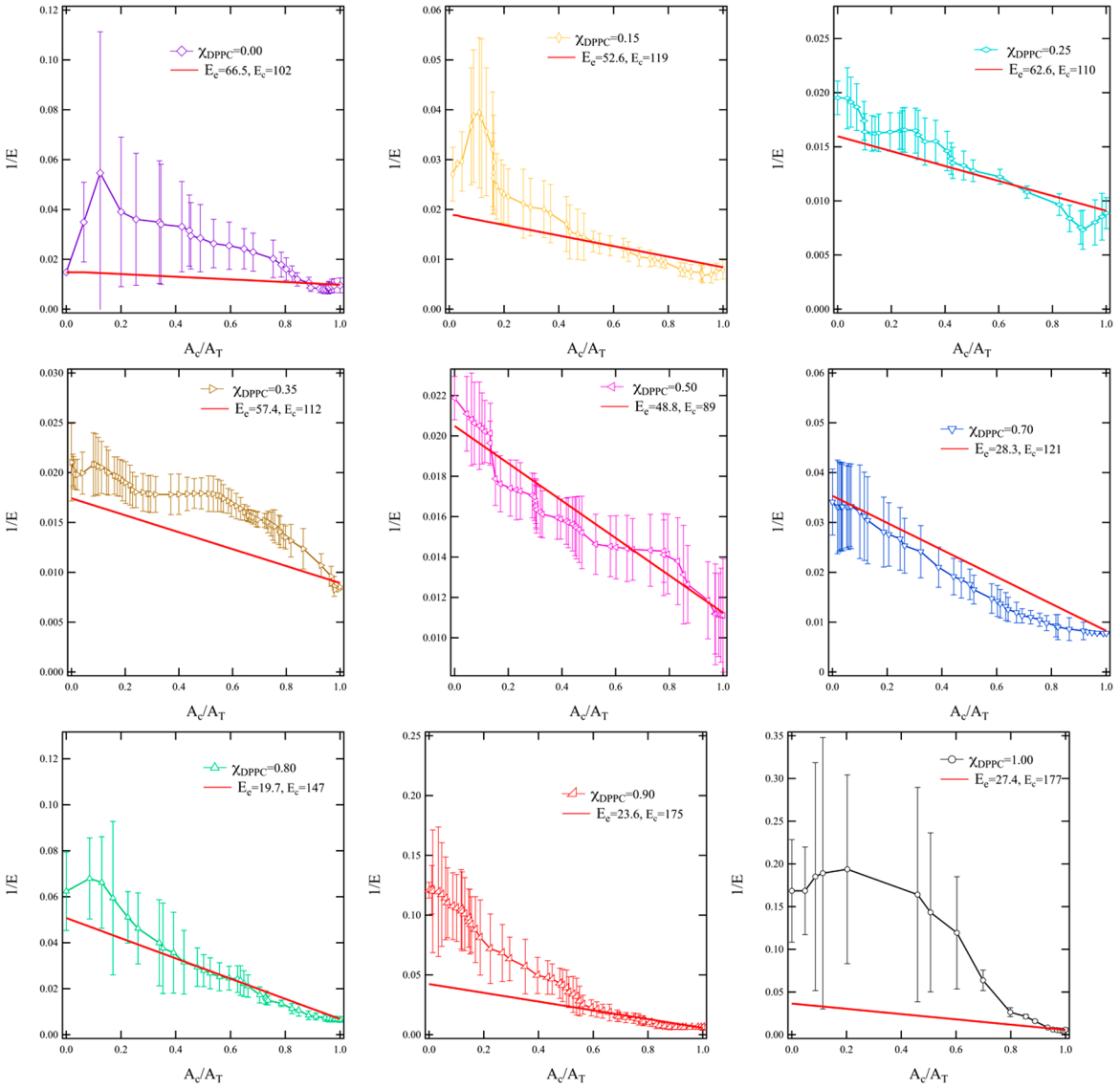

Figure 7. Compressibility as a function of the condensed area to total area ratio: red line: calculated from eq 7 and the parameters of Table 2; experimental points is data extracted from Figure 9 and BAM images.

less packed probably by repulsion between lipids or other contributions may occur, such as disorder of the carbon chains. If there is an excess of area available for each molecule, it might explain the highest compressibility observed in $\chi_{DPPC} \approx 0.5$. However, for $\Pi = 30$ mN/m, the inverse effect occurs, the area is below the predicted for an ideal mixture, it suggests that the molecules are attracted and forms a more compact monolayer, and the monolayer is less compressible, since there is less available free space for the lipids to be compressed. Finally, at higher surface pressure, $\Pi = 40$ mN/m, the dependency of the area is similar to an ideal mixture. A deeper understanding of this optimum packing could be achieved with molecular simulations in the future.

Interfacial Shear Rheology. We also investigated the mechanical behavior of nonhomogeneous monolayers under sinusoidal shear deformations in a range of angular frequencies (0.13−10 s^{-1}). In Figure 10, we show the shear interfacial storage modulus (G') and the shear interfacial loss modulus (G'') as a function of χ_{DPPC}.

The behavior of the mixed monolayers is similar for all the three surface pressures. The monolayer mechanical behavior at low χ_{DPPC} is fluidlike, with $G' \sim 0$. For higher χ_{DPPC}, G' is larger, but smaller than G'' except in the vicinity of $\chi_{DPPC} = 0.5$: the layer behaves as a viscoelastic fluid. This behavior changes to that of a viscoelastic solid around $\chi_{DPPC} = 0.5$, where G' slightly greater than G'' and both are nonzero. Close to $\chi_{DPPC} = 1$, both G' and G'' no longer change appreciably and have the largest values. This behavior is consistent with the percolation effect reported before with condensed area ~0.9. Minima of G'' are visible close to $\chi_{DPPC} \sim 0.5$ where the monolayers are the most compressible. These monolayers are the most loosely packed (the more compressible ones), and hence, their shear viscosity is likely smaller for this reason. The reason why G' is larger than G'' at this point is less obvious. An optimum packing could possibly generate attraction between molecules at the surface and result in a viscoelastic solid, possibly a two-dimensional gel. Overall, the shear viscosities $\eta_s = G''/\omega$ are quite small: with $\omega = 0.13$ s^{-1}, η_s ranges between 0.01 and 1 mN·s/m, with the highest values being obtained for DPPC which is in the LC phase at the pressures investigated in this study.

DOI: 10.1021/acs.langmuir.9b02995
Langmuir 2019, 35, 16734−16744

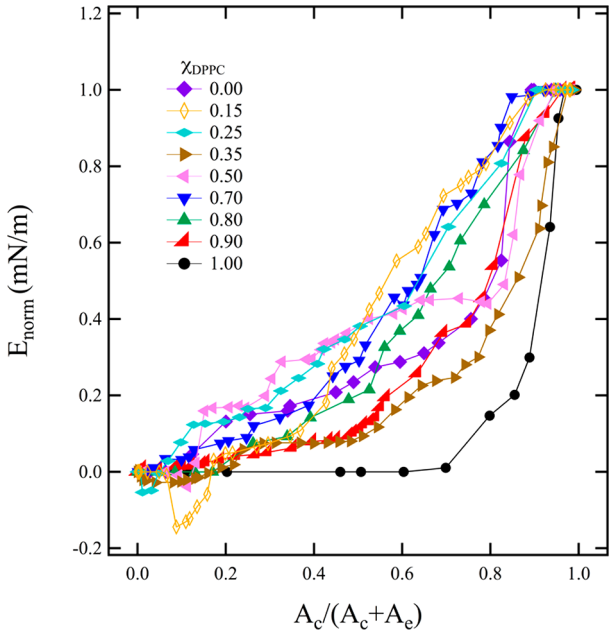

Figure 8. Normalized compression modulus (E_{norm}) as a function of the percentage of the condensed area.

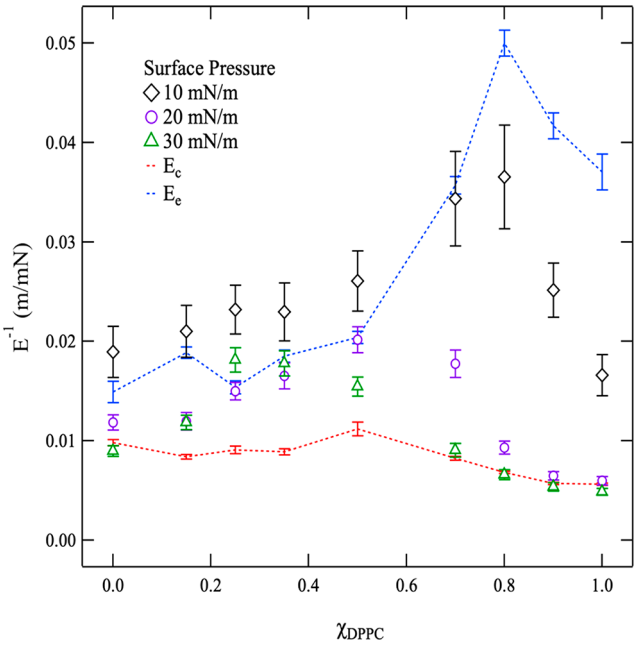

Figure 9. Surface compressibility as a function of DPPC molar fraction at three different surface pressures. The dashed lines correspond to the compressibility at the phase transitions Π_e and Π_c as taken from Table 1.

Wilke et al.,[13] measured the diffusion coefficient D of beads and domains in DMPC-DSPC mixed monolayers at Π = 10 mN/m and used the data to evaluate the surface shear viscosity. The results depend strongly on the model used in the calculation. In our work we measured the interfacial shear viscosity with the magnetic needle method, where the mechanical model used to obtain the viscosity is more straightforward. The model has been carefully validated using measurements of the velocity profile around the needle and it has been shown to be accurate for many different types of monolayers.[46]

We compared our results with those of Sachan et al.[11] who used a similar method (magnetic button instead of needle). They found that the viscosity increases with the area fraction of domains ϕ and is well represented by a Krieger formula for spheres[29,47] assumed to remain valid for discs:

$$\eta_S = \frac{\eta_{S0}}{\left(1 - \frac{\phi}{\phi_p}\right)^2} \quad (9)$$

where ϕ_p is the area fraction for random close packing and η_{S0} is the viscosity limit for vanishing ϕ. In our experiments, $\phi = A_c/(A_c + A_e)$ and ϕ_p is the area fraction at the percolation threshold. Figure 11 shows the viscosity data taken in the phase coexistence region plotted versus $1 - \phi/\phi_p$.

As in ref 11, part of the data follows eq 9, with a limit η_{S0} that increases slightly with surface pressure. Two exceptions are noticeable: the viscosity of the layers with χ_{DPPC} = 0.5 and 1 are smaller, as expected in view of the viscosity behavior in Figure 10: the viscosity shows a minimum for χ_{DPPC} = 0.5 and decreases when χ_{DPPC} approaches 1. The behavior predicted by eq 9 is therefore not general and depends of additional molecular details (possibly on the shape of the domains and on their interactions).

CONCLUSIONS

In this study, we reported the impact of the addition of POPE in DPPC monolayers on their mechanical properties. We found that the LE−LC coexistence phase of pure DPPC shifts to higher surface pressures as the POPE molar fraction increases in the monolayer as corroborated by the BAM images. As in other lipid systems, the surface pressure is not constant in the LE−LC coexistence region. The compression elastic modulus increases with the amount of LC phase, but less than predicted by a simple effective medium model. The differences arise from the fact that, upon compression, the domains grow at a rate faster than the compression rate, but not fast enough to reach thermodynamic equilibrium, in which case the modulus should be zero. Before reaching the LC phase, the condensed phase percolates and the modulus no

Table 3. Percolation Thresholds in Percentage of Condensed Phase for Different DPPC Molar Fractions and Determined Either from the Images or from the Saturation of the Elastic Modulus

	χ_{DPPC}								
	0	0.15	0.25	0.35	0.5	0.7	0.8	0.9	1
percolation threshold from BAM images	0.84 ± 0.06	0.85 ± 0.06	0.85 ± 0.04	0.86 ± 0.06	0.92 ± 0.03	0.88 ± 0.05	0.92 ± 0.04	0.94 ± 0.02	0.95 ± 0.02
percolation threshold from elastic moduli (Figure 8)	0.79 ± 0.06	0.78 ± 0.07	0.76 ± 0.07	0.87 ± 0.05	0.88 ± 0.03	0.82 ± 0.03	0.89 ± 0.03	0.98 ± 0.02	0.998 ± 0.02

DOI: 10.1021/acs.langmuir.9b02995
Langmuir 2019, 35, 16734−16744

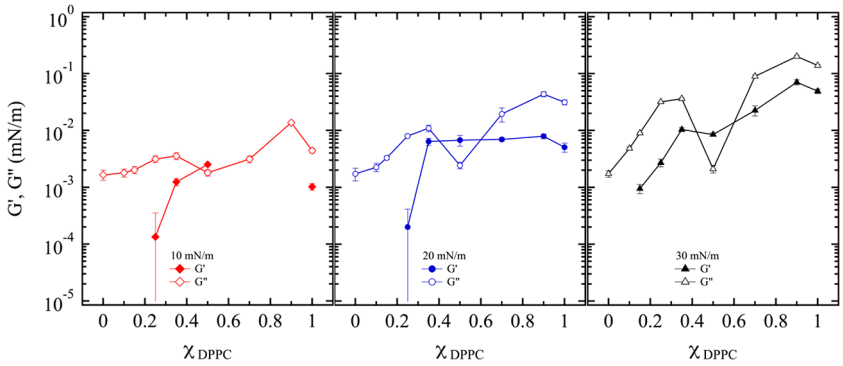

Figure 10. Interfacial shear storage (G') and loss modulus (G'') as a function of DPPC molar fraction at three different surface pressures. The lines are guides for the eye. The experimental error bars are smaller than the symbol size in some cases.

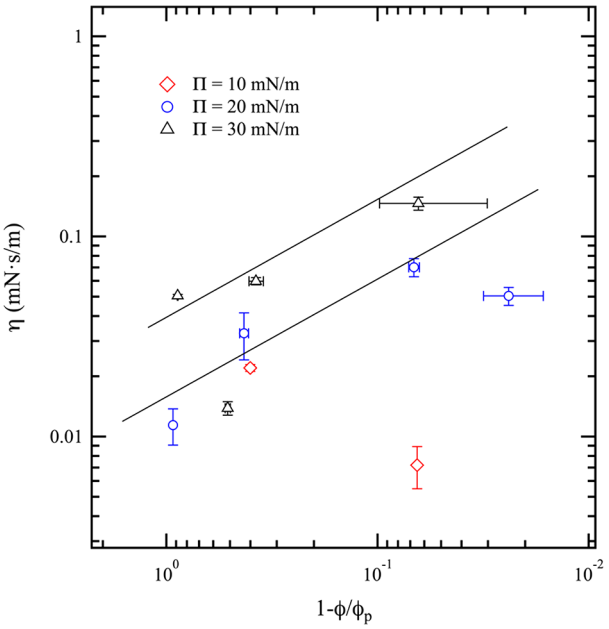

Figure 11. Interfacial shear viscosity as a function of $1 - \phi/\phi_p$ (eq 9) of POPE−DPPC mixed monolayers for three constant surface pressures in the LE−LC phase coexistence region. The two lowest points on the left correspond to $\chi_{DPPC} = 0.5$ and the two lowest points on the right to $\chi_{DPPC} = 1$. The lines are predictions from eq 9, and their slope is equal to 2.

longer change significantly. The percolation threshold is quite high, suggesting repulsive interactions between domains. The behavior of the shear moduli is consistent with these findings.

We observed a change in the form of the domains in the coexistence region around $\chi_{DPPC} = 0.5$, that could possibly be related to a change of the line tension. Around this composition, the kink in the $\Pi(a)$ curve vanishes and both the compression modulus and the shear loss modulus is minimum when the surface pressure is large enough. This behavior could be due to an optimum in molecular packing. Measurements of the time dependence of the mechanical properties, performed using oscillating shear and compression with variable frequencies are currently underway, in order to clarify further this complex mechanical behavior.

To summarize our original findings: we explained the compression behavior of the phase separated domains in the mixed monolayers by a dependence of the mechanical response upon the velocity of compression. Domain percolation seems to be a general feature, the percolation concentration giving information about the interactions between domains. The mechanical behavior upon compression and shear were found to be correlated.

These results are an important step that will help to better understand the behavior of biological membranes. These membranes contain not only different types of lipids, but also proteins and small molecules such as cholesterol. There is nowadays a considerable activity on lipid rafts that are nothing else than phase separated lipid bilayers and where proteins tend to segregate, facts which seem quite important for the understanding of membrane function.[48] Clarifying the phase separation process in layers is therefore an important goal.

■ ASSOCIATED CONTENT

Supporting Information

The Supporting Information is available free of charge at https://pubs.acs.org/doi/10.1021/acs.langmuir.9b02995.

Isotherms of POPE monolayers for different times after spreading on the air−water interface, BAM images obtained at different surface pressures spanned in the studied DPPC molar fractions, surface pressure at the kink of the isotherms and the surface pressure at the onset of the liquid expanded phase as observed with BAM, expanded area to condensed area ratio as a function of χ_{DPPC} at Π = 15, 25, 30, and 35 mN/m, Gibbs excess free energy for different surface pressures as a function of the monolayer composition, and procedure followed for BAM images analysis to determine condensed and expanded areas (PDF)

■ AUTHOR INFORMATION

Corresponding Author

*E-mail: gabriel.espinosa@umich.mx.

ORCID

Rolando Castillo: 0000-0001-6331-0311

Gabriel Espinosa: 0000-0003-2581-4273

Notes

The authors declare no competing financial interest.

■ ACKNOWLEDGMENTS

We are grateful to Francisco Monroy and Jean-Pierre Hulin for useful suggestions concerning the application of effective medium models. This work was supported by CONACYT Ciencia Basica program Grants CB-2013/220331 to G.E. and CB-2012/182526 to J.C.-T. G.E. acknowledges CIC-UMSNH

DOI: 10.1021/acs.langmuir.9b02995
Langmuir 2019, 35, 16734−16744

for annual grants. A.S.L. was supported by CONACYT doctoral scholarship. The authors are grateful to CONACYT Mexican Soft Matter Network. We thank Salvador Ramos for technical assistance with the BAM experiments.

REFERENCES

(1) Mouritsen, O. G. *Life - As a Matter of Fat*; Springer, 2004.
(2) Sprong, H.; van der Sluijs, P.; van Meer, G. How Proteins Move Lipids and Lipids Move Proteins. *Nat. Rev. Mol. Cell Biol.* **2001**, *2* (7), 504−513.
(3) Zhang, Y. L.; Matar, O. K.; Craster, R. V. Analysis of Tear Film Rupture: Effect of Non-Newtonian Rheology. *J. Colloid Interface Sci.* **2003**, *262* (1), 130−148.
(4) Marsh, D. Lateral Pressure in Membranes. *Biochim. Biophys. Acta, Rev. Biomembr.* **1996**, *1286* (3), 183.
(5) Yokoi, N.; Yamada, H.; Mizukusa, Y.; Bron, A. J.; Tiffany, J. M.; Kato, T.; Kinoshita, S. Rheology of Tear Film Lipid Layer Spread in Normal and Aqueous Tear−Deficient Dry Eyes. *Invest. Ophthalmol. Visual Sci.* **2008**, *49* (12), 5319.
(6) Caruso, B.; Mangiarotti, A.; Wilke, N. Stiffness of Lipid Monolayers with Phase Coexistence. *Langmuir* **2013**, *29* (34), 10807−10816.
(7) Gaines, G. L. *Insoluble Monolayers at Liquid-Gas Interfaces*; John Wiley & Sons Inc, 1966.
(8) Pallas, N. R.; Pethica, B. A. Liquid-Expanded to Liquid-Condensed Transitions in Lipid Monolayers at the Air/Water Interface. *Langmuir* **1985**, *1* (4), 509−513.
(9) Arriaga, L. R.; López-Montero, I.; Ignés-Mullol, J.; Monroy, F. Domain-Growth Kinetic Origin of Nonhorizontal Phase Coexistence Plateaux in Langmuir Monolayers: Compression Rigidity of a Raft-Like Lipid Distribution. *J. Phys. Chem. B* **2010**, *114* (13), 4509−4520.
(10) Bornert, M.; Bretheau, T.; Gilormini, P. *Homogenization in Mechanics of Materials*; ISTE, 2008.
(11) Sachan, A. K.; Choi, S. Q.; Kim, K. H.; Tang, Q.; Hwang, L.; Lee, K. Y. C.; Squires, T. M.; Zasadzinski, J. A. Interfacial Rheology of Coexisting Solid and Fluid Monolayers. *Soft Matter* **2017**, *13* (7), 1481−1492.
(12) Espinosa, G.; López-Montero, I.; Monroy, F.; Langevin, D. Shear Rheology of Lipid Monolayers and Insights on Membrane Fluidity. *Proc. Natl. Acad. Sci. U. S. A.* **2011**, *108* (15), 6008−6013.
(13) Wilke, N.; Vega Mercado, F.; Maggio, B. Rheological Properties of a Two Phase Lipid Monolayer at the Air/Water Interface: Effect of the Composition of the Mixture. *Langmuir* **2010**, *26* (13), 11050−11059.
(14) Harayama, T.; Riezman, H. Understanding the Diversity of Membrane Lipid Composition. *Nat. Rev. Mol. Cell Biol.* **2018**, *19* (5), 281−296.
(15) Schroeder, R.; London, E.; Brown, D. Interactions between Saturated Acyl Chains Confer Detergent Resistance on Lipids and Glycosylphosphatidylinositol (GPI)-Anchored Proteins: GPI-Anchored Proteins in Liposomes and Cells Show Similar Behavior. *Proc. Natl. Acad. Sci. U. S. A.* **1994**, *91* (25), 12130−12134.
(16) Krägel, J.; Kretzschmar, G.; Li, J. B.; Loglio, G.; Miller, R.; Möhwald, H. Surface Rheology of Monolayers. *Thin Solid Films* **1996**, *284−285* (1), 361−364.
(17) Möhwald, H. Phospholipid and Phospholipid-Protein Monolayers at the Air/Water Interface. *Annu. Rev. Phys. Chem.* **1990**, *41*, 441−476.
(18) Kim, K.; Choi, S. Q.; Zasadzinski, J. A.; Squires, T. M. Interfacial Microrheology of DPPC Monolayers at the Air−Water Interface. *Soft Matter* **2011**, *7* (17), 7782.
(19) Bringezu, F.; Ding, J.; Brezesinski, G.; Zasadzinski, J. A. Changes in Model Lung Surfactant Monolayers Induced by Palmitic Acid. *Langmuir* **2001**, *17* (15), 4641−4648.
(20) Rawicz, W.; Olbrich, K. C.; McIntosh, T.; Needham, D.; Evans, E. Effect of Chain Length and Unsaturation on Elasticity of Lipid Bilayers. *Biophys. J.* **2000**, *79* (1), 328−339.
(21) Ahn, T.; Yun, C.-H. H. Phase Properties of Liquid-Crystalline Phosphatidylcholine/Phosphatidylethanolamine Bilayers Revealed by Fluorescent Probes. *Arch. Biochem. Biophys.* **1999**, *369* (2), 288−294.
(22) Dawaliby, R.; Trubbia, C.; Delporte, C.; Noyon, C.; Ruysschaert, J. M.; Van Antwerpen, P.; Govaerts, C. Phosphatidylethanolamine Is a Key Regulator of Membrane Fluidity in Eukaryotic Cells. *J. Biol. Chem.* **2016**, *291* (7), 3658−3667.
(23) Malcharek, S.; Hinz, A.; Hilterhaus, L.; Galla, H.-J. Multilayer Structures in Lipid Monolayer Films Containing Surfactant Protein C: Effects of Cholesterol and POPE. *Biophys. J.* **2005**, *88* (4), 2638−2649.
(24) Volinsky, R.; Cwiklik, L.; Jurkiewicz, P.; Hof, M.; Jungwirth, P.; Kinnunen, P. K. J. Oxidized Phosphatidylcholines Facilitate Phospholipid Flip-Flop in Liposomes. *Biophys. J.* **2011**, *101* (6), 1376−1384.
(25) Voss, L. F.; Bazerbashi, M. F.; Beekman, C. P.; Hadad, C. M.; Allen, H. C. Oxidation of Oleic Acid at Air/Liquid Interfaces. *J. Geophys. Res.* **2007**, *112* (6), 1−9.
(26) Brooks, C. F.; Fuller, G. G.; Frank, C. W.; Robertson, C. R. An Interfacial Stress Rheometer To Study Rheological Transitions in Monolayers at the Air-Water Interface. *Langmuir* **1999**, *15* (7), 2450−2459.
(27) Ding, J.; Warriner, H. E.; Zasadzinski, J. A.; Schwartz, D. K. Magnetic Needle Viscometer for Langmuir Monolayers. *Langmuir* **2002**, *18* (7), 2800−2806.
(28) Naumann, C. A.; Brooks, C. F.; Knoll, W.; Fuller, G. G.; Frank, C. W. Viscoelastic Properties of Lipopolymers at the Air-Water Interface: A Combined Interfacial Stress Rheometer and Film Balance Study. *Langmuir* **1999**, *15* (13), 7752−7761.
(29) Macosko, C. W. *Rheology: Principles, Measurements and Applications*; Wiley, 1996; Vol. *86*.
(30) Jyoti, A.; Prokop, R. M.; Li, J.; Vollhardt, D.; Kwok, D. Y.; Miller, R.; Möhwald, H.; Neumann, A. W. An Investigation of the Compression Rate Dependence on the Surface Pressure-Surface Area Isotherm for a Dipalmitoyl Phosphatidylcholine Monolayer at the Air/Water Interface. *Colloids Surf., A* **1996**, *116* (1−2), 173−180.
(31) Rey Gómez-Serranillos, I.; Miñones, J.; Dynarowicz-Łątka, P.; Miñones, J.; Conde, O. Surface Behavior of Oleoyl Palmitoyl Phosphatidyl Ethanolamine (OPPE) and the Characteristics of Mixed OPPE-Miltefosine Monolayers. *Langmuir* **2004**, *20* (26), 11414−11421.
(32) Albrecht, O.; Gruler, H.; Sackmann, E. Polymorphism of Phospholipid Monolayers. *J. Phys. (Paris)* **1978**, *39* (3), 301−313.
(33) Broniatowski, M.; Mastalerz, P.; Flasiński, M. Studies of the Interactions of Ursane-Type Bioactive Terpenes with the Model of Escherichia Coli Inner Membrane - Langmuir Monolayer Approach. *Biochim. Biophys. Acta, Biomembr.* **2015**, *1848* (2), 469−476.
(34) Mcconlogue, C. W.; Vanderlick, T. K. A Close Look at Domain Formation in DPPC Monolayers. *Langmuir* **1997**, *13* (26), 7158−7164.
(35) Li, J. B.; Miller, R.; Vollhardt, D.; Möhwald, H. Spreading Concentration Effect on the Morphology of Phospholipid Monolayers. *Thin Solid Films* **1998**, *327−329*, 84−86.
(36) Gutierrez-Campos, A.; Diaz-Leines, G.; Castillo, R. Domain Growth, Pattern Formation, and Morphology Transitions in Langmuir Monolayers. A New Growth Instability. *J. Phys. Chem. B* **2010**, *114* (15), 5034−5046.
(37) Bruinsma, R.; Rondelez, F.; Levine, A. Flow-Controlled Growth in Langmuir Monolayers. *Eur. Phys. J. E: Soft Matter Biol. Phys.* **2001**, *6* (3), 191−200.
(38) Krüger, P.; Lösche, M. Molecular Chirality and Domain Shapes in Lipid Monolayers on Aqueous Surfaces. *Phys. Rev. E: Stat. Phys., Plasmas, Fluids, Relat. Interdiscip. Top.* **2000**, *62* (5), 7031−7043.
(39) Schneider, C. A.; Rasband, W. S.; Eliceiri, K. W. NIH Image to ImageJ: 25 Years of Image Analysis. *Nat. Methods* **2012**, *9* (7), 671.
(40) Costin, I. S.; Barnes, G. T. Two-Component Monolayers. II. Surface Pressure-Area Relations for the Octadecanol-Docosyl Sulphate System. *J. Colloid Interface Sci.* **1975**, *51* (1), 106−121.

DOI: 10.1021/acs.langmuir.9b02995
Langmuir 2019, 35, 16734−16744

(41) Gradella Villalva, D.; Diociaiuti, M.; Giansanti, L.; Petaccia, M.; Bešker, N.; Mancini, G. Molecular Packing in Langmuir Monolayers Composed of a Phosphatidylcholine and a Pyrene Lipid. *J. Phys. Chem. B* **2016**, *120* (6), 1126−1133.
(42) Mertens, S.; Moore, C. Continuum Percolation Thresholds in Two Dimensions. *Phys. Rev. E - Stat. Nonlinear, Soft Matter Phys.* **2012**, *86* (6), 061109.
(43) Israelachvili, J. N.; Mitchell, D. J.; Ninham, B. W. Theory of Self-Assembly of Lipid Bilayers and Vesicles. *Biochim. Biophys. Acta, Biomembr.* **1977**, *470* (2), 185−201.
(44) Israelachvili, J. N. Physical Principles and Modes of Interaction of Membrane Lipids and Amphiphiles. In *Chemistry and Biological Activities of Bacterial Surface Amphiphiles*; Elsevier, 1981; pp 119−123.
(45) van Meer, G.; Voelker, D. R.; Feigenson, G. W. Membrane Lipids: Where They Are and How They Behave. *Nat. Rev. Mol. Cell Biol.* **2008**, *9* (2), 112−124.
(46) Reynaert, S.; Brooks, C. F.; Moldenaers, P.; Vermant, J.; Fuller, G. G. Analysis of the Magnetic Rod Interfacial Stress Rheometer. *J. Rheol. (Melville, NY, U. S.)* **2008**, *52* (1), 261−285.
(47) Ding, J.; Warriner, H. E.; Zasadzinski, J. A. Viscosity of Two-Dimensional Suspensions. *Phys. Rev. Lett.* **2002**, *88* (16), 168102.
(48) Lingwood, D.; Simons, K. Lipid Rafts As a Membrane-Organizing Principle. *Science (Washington, DC, U. S.)* **2010**, *327* (5961), 46−50.

DOI: 10.1021/acs.langmuir.9b02995
Langmuir 2019, 35, 16734−16744